Anisotropic spatial structure of deep acceptor states in GaAs and GaP

Please check the document version of this publication:

• A submitted manuscript is the version of the article upon submission and before peer-review. There can be important differences between the submitted version and the official published version of record. People interested in the research are advised to contact the author for the final version of the publication, or visit the DOI to the publisher's website.
• The final author version and the galley proof are versions of the publication after peer review.
• The final published version features the final layout of the paper including the volume, issue and page numbers.

[Link to publication](#)

Anisotropic spatial structure of deep acceptor states in GaAs and GaP

C. Çelebi, P. M. Koenraad, and A. Yu. Silov

*COBRA Inter-University Research Institute, Department of Applied Physics, Eindhoven University of Technology, P.O. Box 513,
NL-5600 MB Eindhoven, The Netherlands*

W. Van Roy

IMEC, Kapeldreef 75, B-3001 Leuven, Belgium

A. M. Monakhov

Ioffe Physico-Technical Institute, 26 Polytekhnicheskaya, St. Petersburg 194021, Russian Federation

J.-M. Tang

Department of Physics, University of New Hampshire, Durham, New Hampshire 03824, USA

M. E. Flatté

Optical Science and Technology Center and Department of Physics and Astronomy, University of Iowa, Iowa City, Iowa 52242, USA

Cross-sectional scanning tunneling microscopy is used to identify the origin of the anisotropic electronic structure of acceptor states in III–V semiconductors. The density of states introduced by a hole bound to an individual Cd acceptor in GaP is spatially mapped at room temperature. Similar to the Mn hole wave function in GaAs, we found a highly anisotropic, crosslike shape of the hole bound to Cd both at the GaP(110) and the GaP($1\bar{1}0$) orthogonal cleavage planes. The experimentally observed similarity of the symmetry properties of Mn:GaAs to Cd:GaP shows that the anisotropic structure of acceptor states in zinc-blende III–V compounds is determined by the cubic symmetry of the host crystal. Nevertheless, the weak spin-orbit interaction in GaP leads to a slight modification of the Cd bound-hole wave function relative to that of Mn in GaAs. In addition to the anisotropic angular structure of the d-like spherical harmonic of the wave function, which dominates the appearance of the hole ground state far from the ionic core, the admixture of g-like and higher order spherical harmonics is identified at the sides of the Cd hole wave function. The experimentally obtained results agree with both atomistic tight-binding and envelope-function effective-mass theoretical models.

PACS number(s): 71.55.Eq, 75.50.Pp, 68.37.Ef, 71.15.−m

I. INTRODUCTION

Dopant atoms are essential components in semiconductor materials not only because they provide extrinsic charges or magnetic moments, but because single dopants offer the potential to be used as the functional parts of nanoscale or quantum information devices.[1–4] In order to utilize single dopants in such devices, their electronic and magnetic properties have to be understood in detail, including the influence of the host materials. This includes the spin-orbit (SO) interaction, which in bulk semiconductors doped with magnetic atoms is known to be responsible for magnetic anisotropy and optical dichroism.[5] Cross-sectional scanning tunneling microscopy (X-STM), with its high spatial resolution and electronic sensitivity, has recently become a sophisticated technique to investigate at the atomic scale the local electronic structure of individual dopants on the cleavage surface of cubic III–V compounds.

In X-STM measurements, donors like Si in GaAs appear as isotropic round protrusions, in analogy with the hydrogenic impurity model,[6] whereas relatively deep acceptors like Mn introduce a distinct anisotropic contrast in GaAs.[7] A multitude of experimental techniques, including electron paramagnetic resonance[8] and infrared (IR) spectroscopy,[9] revealed the existence of a Mn-related neutral $A^0(d^5+\text{hole})$

acceptor center in GaAs. Although the IR spectroscopy data were analyzed theoretically within a spherical approximation for the electronic structure,[9] a large contribution of the anisotropic d-like spherical harmonic to the bound-hole ground state was identified experimentally by X-STM measurements.[7] Similar results have since been found for the shallower Mn in InAs.[10] Under appropriate tunnel conditions, Mn reveals a striking anisotropic crosslike shape of the local density of states (LDOS) with a twofold symmetry on the GaAs(110) cleavage plane. The contrast introduced by Mn exhibits a weakly asymmetric profile along the GaAs[001] crystal direction and a slight reduction of the spatial symmetry across the single GaAs($1\bar{1}0$) mirror plane. The lowering of the contrast symmetry may be related to the symmetry properties of the crystal lattice at the GaAs(110) cleavage surface.

Theoretical approaches based on an atomistic tight-binding model (TBM) and an envelope-function effective-mass model (EMM) have provided insight into the origin of the anisotropic ground state wave function of a valence hole bound to an individual Mn center in GaAs.[7,11] In EMM, the acceptor state wave function is described analytically. It provides a detailed qualitative insight into the composition of the wave functions as a mixture of the different spherical harmonics due to the cubic GaAs environment. The TBM

takes into account the full band dispersion and models the local binding potential of a tetrahedral symmetry due to the specific bonding configuration of the dopant atom in the host crystal. The TBM provides quantitative information on the atomic scale and allows a direct comparison with the experimental X-STM results. It is known that the *d*-like spherical harmonic of the hole ground state originates from the strong hybridization of the Mn $3d^5$ electrons with the As *p* states associated predominantly with the host heavy-hole band. Whether or not the SO interaction in GaAs is included, TBM calculations find an anisotropic wave function for the Mn acceptor state similar to that seen experimentally.[7] Further TBM calculations including the SO interaction revealed a small spin orientation dependence of the LDOS around an isolated Mn dopant in GaAs.[12] Within the EMM, the anisotropy in the bulklike (Mn²⁺3d⁵+hole) acceptor state was traced to the influence of the cubic symmetry of the GaAs crystal, which enhances the contribution of the *d*-like spherical harmonics of the hole ground state.

In this work, we present a comprehensive experimental and theoretical investigation of the role of the SO interaction and the cubic crystal symmetry on the spatial structure of relatively deep acceptors. We first focus on our experimental X-STM data of the spatial dependence of the Mn state in GaAs and the Cd state in GaP. The principal difference between these two host materials is that GaP has a much smaller SO interaction than GaAs. The anisotropic structure of each acceptor will be analyzed individually and compared quantitatively with each other with an emphasis on differences in symmetry. The interpretation of the experimental measurements of the acceptor ground state wave function for both Mn:GaAs and Cd:GaP will be evaluated in detail by the TBM and by the EMM within the cubic approximation.

II. EXPERIMENTAL APPROACH

To study experimentally the effect of SO interaction on the acceptor shape anisotropy, we carried out a set of X-STM measurements on Mn acceptors in GaAs and on Cd acceptors in GaP. We evaluate the relative SO interaction by considering the energetic position of the split-off band (ΔE_{so}) relative to the acceptor ground state binding energy $E_a(1S_{3/2})$ in the band gap region. Although the Cd acceptor binding energy of $E_a=102$ meV in GaP is nearly identical to that of Mn in GaAs ($E_a=113$ meV), the SO interaction differs greatly between the two hosts. The value of $\delta=\Delta E_{so}/E_a(1S_{3/2})$ for a specific dopant and host material qualitatively determines whether the dopant is in the weak SO coupling limit ($\delta \ll 1$) or strong SO coupling limit ($\delta \gg 1$).[13] As measured from the top of the valence band, the magnitude of the SO interaction in GaP, $\Delta E_{so}(GaP)=80$ meV, is about four times smaller than that of GaAs, $\Delta E_{so}(GaAs)=340$ meV.[14] Thus, $\delta_{Cd:GaP}<1$, and $\delta_{Mn:GaAs}>1$, and $\delta_{Mn:GaAs}\sim 4\delta_{Cd:GaP}$.

The room temperature X-STM measurements were performed at the atomic scale individually on *p*-type and nondegenerate Mn doped GaAs and Cd doped GaP samples. In order to achieve a clean and atomically flat surface, the samples were cleaved *in situ* under ultrahigh vacuum conditions ($<2\times10^{-11}$ mbar) and the experiments were done by
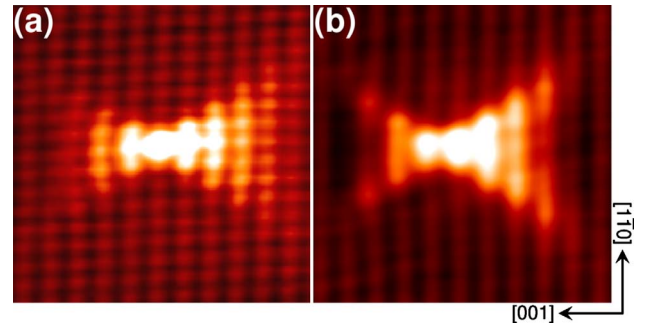

FIG. 1. (Color online) Magnified X-STM topography image of a single (a) Mn acceptor in GaAs and (b) Cd acceptor in GaP located near the (110)-cleavage surface plane. The measurement set points for Mn:GaAs are $U_s=+0.7$ V and $I_t=50$ pA, and for Cd:GaP are $U_s=+1.4$ V and $I_t=50$ pA. The size of each frame is 6×6 nm².

using electrochemically prepared polycrystalline tungsten tips. The first set of measurements was carried out on the (110) surface plane of a 150 nm thick molecular-beam-epitaxy-grown Mn doped GaAs layer with a doping concentration of about 2×10^{18} cm⁻³. For the other set, two liquid-encapsulated-Czochralski-grown, Cd doped GaP samples, with a doping level of about 5×10^{17} cm⁻³, were measured separately on the two nonequivalent (110) and (1̄10) surface planes of orthogonally cleaved crystal facets. These two planes exhibit perpendicular cross sections through the crystal, in which the orientations of the Ga and As zigzag atomic rows are inverted relative to each other. The concentration of the dopants in the respective crystals was intentionally set to a low value during the growth to avoid impurity-impurity interaction and impurity band formation. The cleaved sample surface planes were scanned with a wide range of applied voltages in constant current mode, during which the empty state topography and the current images were recorded simultaneously.

III. EXPERIMENTAL RESULTS AND DISCUSSION

In Fig. 1, we compare the atomically resolved X-STM topography maps of the hole distribution around isolated Mn and Cd acceptors in GaAs and GaP materials, respectively. The measurement for Mn:GaAs was acquired at a sample bias of $U_s=+0.7$ V in constant current imaging mode. At this relatively small sample bias, where the Fermi level of the STM tip is moved far below the bottom of the conduction band, it becomes possible to image the occupied As states as well as the electronic contrast introduced by deeply buried Mn atoms located at least 10 ML (monolayer) below the cleavage plane or closer to the surface. As can be seen in Fig. 1(a), Mn introduces a typical crosslike LDOS with a twofold symmetry on the GaAs surface. Unlike the previously reported triangular contrast for shallow Cd acceptor in GaAs ($E_a=35$ meV),[15] we found a spatially extended, highly anisotropic crosslike electronic structure for Cd in GaP [Fig. 1(b)]. The shape, orientation, and the symmetry properties of Cd closely resemble the anisotropic structure of the (Mn²⁺ 3d⁵+hole) complex projected on a GaAs surface.
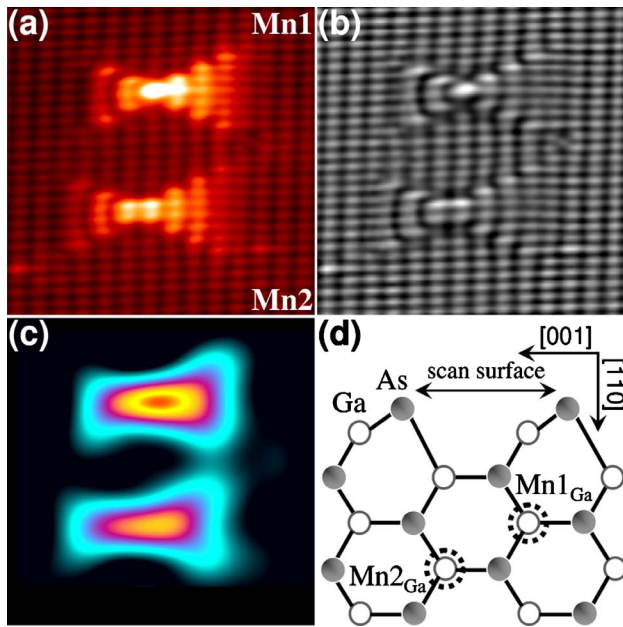
FIG. 2. (Color online) X-STM (a) topography, (b) atomic corrugation, and (c) envelope images of two neighboring Mn dopants located at two different subsurface planes below the GaAs(110) cleavage surface. Each of the Mn atom introduces a distinct contrast on the atomic LDOS of the As sublattice. The size of each frame is 8×8 nm². (d) Schematic view of the GaAs($1\bar{1}0$) cross-sectional plane representing the Mn on Ga site located at either odd (Mn1) or even (Mn2) sublattice position.

Similar to Mn:GaAs, Cd is symmetric across the ($1\bar{1}0$) reflection plane and displays a weak asymmetry along the [001] crystal direction. This symmetry is C_s, but we will refer to images such as Fig. 1(b) as showing a slightly reduced C_{2v} symmetry with the surface normal as symmetry axis. The only difference observed between the topography of the two acceptors is the lateral size of the corresponding contrasts. For example, Mn-induced LDOS extends spatially over a few atomic distances more than the one for Cd. This is due to the fact that each dopant is located at a different geometric depth with respect to the cleavage surface plane.

In order to determine the actual subsurface depth and the spatial position of the dopants with monolayer precision, we analyzed the relative intensity of the electronic contrast of all the observed acceptor features with respect to the atomic corrugation of the surface states. Based on the spatial symmetry of the crosslike features, we distinguished Mn and Cd located on a Ga site with a distance of about 7 ± 1 and 4 ± 1 ML below the GaAs(110) and GaP(110) cleavage surfaces, respectively. For the deeper acceptors, the spatial extension of the contrast extends even further along the [001] direction. Our observations clearly show that the anisotropic features introduced by Mn and Cd tend to become more symmetric when the dopant is located deeper inside the host crystal, where the environment is nearer to the bulk host material.

Figure 2(a) shows a magnified X-STM topography map of a pair of Mn dopants (labeled as Mn1 and Mn2) in GaAs. To further explore the spatial symmetry and the anisotropy

of Mn contrast, a Fourier filter [fast Fourier transform (FFT)] is applied to separate the background atomic corrugation of the As atomic sublattice (high-frequency topography component) [Fig. 2(b)] and the Mn related envelopes (low-frequency topography component) [Fig. 2(c)] from the topography map. The symmetry and height analysis obtained from the topography line profiles applied along the GaAs[001] direction (Fig. 4) reveal that Mn1 is located 1 ML closer to the GaAs surface than Mn2; hence Mn1 exhibits a higher intensity and a smaller spatial extension as compared to Mn2 in the topography image. Evident from the high-frequency images [Fig. 2(b)] and topography line profiles [Fig. 4(a)], the two Mn dopants evidence distinct spatial symmetry, appearing as two different arrangements of the atomic LDOS on the As sublattice. The contrast symmetry is reflected in an equal raising of either two As atoms or only a single maximum of one As atom in the vicinity of the Mn center. This is due to the fact that Mn is positioned either in between (i.e., Mn2 at even subsurface plane) or underneath (i.e., Mn1 at odd subsurface plane) the surface Ga atomic rows. Consistent with the zigzag alternation of the adjacent planes in a typical zinc-blende structure, the substitution of the dopant atom alters spatially in Ga sublattice position from one plane to another with respect to the top GaAs(110) cleavage surface [Fig. 2(d)]. Independent of the spatial position of Mn, we also observed a pronounced local distortion of the atomic As LDOS around each Mn center extending along [001] and [00$\bar{1}$] opposite crystallographic directions. This is most probably an electronic effect, because the distortion of the atomic LDOS vanishes when we image the Mn atoms at higher applied voltages.

Although the orientation of the crosslike contrast is always the same for all dopant atoms in one sample, there are crucial differences if we compare (110) and ($1\bar{1}0$) cleavage surfaces. It is known that these two surfaces represent orthogonal cross sections through the crystal. Figure 3 shows that the anisotropic contrast introduced by Cd has a reversed orientation on the GaP($1\bar{1}0$) compared to the GaP(011) surface with respect to the [100] direction. Such inversion of the asymmetric shape is consistent with the opposite crystallographic orientation of the Ga-As zigzag rows along the [$1\bar{1}0$] or [110] direction, which is induced by the natural inversion asymmetry of the ($1\bar{1}0$) and (110) surfaces. The symmetry reversal of the Cd contrast in GaP is in good agreement with recent X-STM results on the inversion of the triangular shape of shallow Zn acceptors on the orthogonal GaAs surface planes.[16]

Based on the symmetry and the height analysis of the Cd contrasts, we identified both Cd centers (labeled as Cd1 and Cd2) to be located in an odd Ga sublattice position at different subsurface depths with an in-plane separation of about 3 ± 1 ML below the GaP cleavage plane. In comparison with the Cd2 contrast on GaP(110) plane, the intensity introduced by Cd1 on GaP($1\bar{1}0$) is relatively high, whereas the respective contrast exhibits a lower spatial extension with a strongly broken symmetry (nearly a triangular shape) along the [00$\bar{1}$] direction. This is due to the relative nearness of Cd1 to the cleavage surface compared to Cd2. For the near-
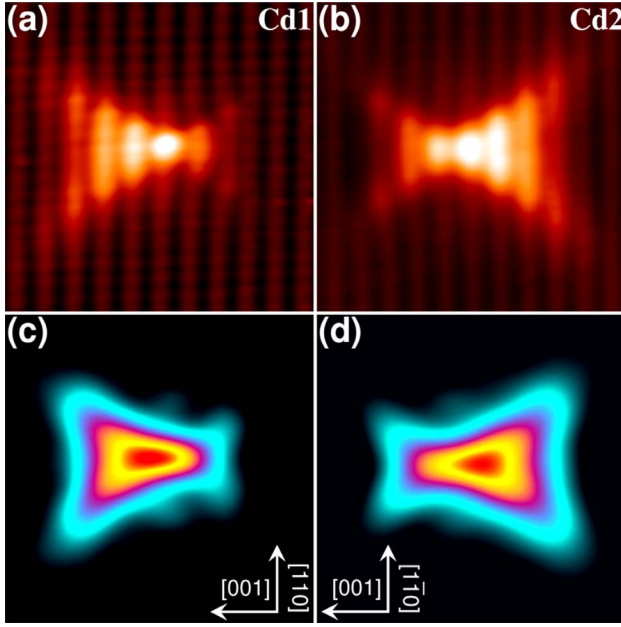
FIG. 3. (Color online) X-STM topography image of a single and isolated Cd acceptor measured at (a) GaP($1\bar{1}0$) and (b) GaP(110) orthogonal surface planes. (c) and (d) depict the corresponding contour plots of the envelope images obtained by low-pass FFT filtering. The measurement set points are $U_s = +1.4$ V and $I_t = 50$ pA for both of the surfaces. The size of each frame is 6×6 nm².
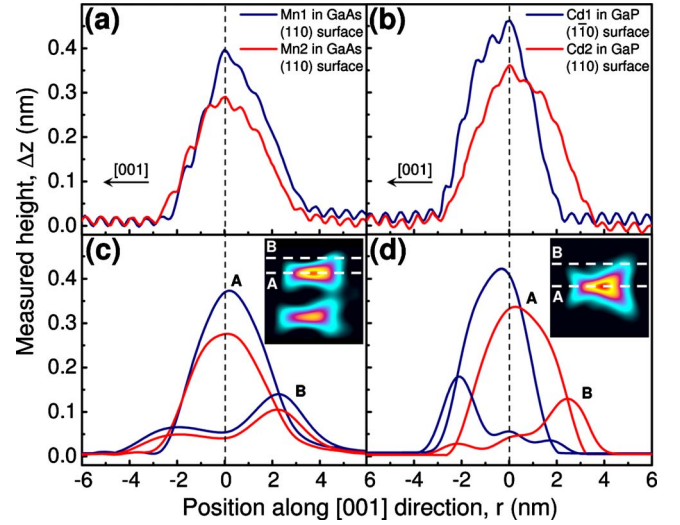

FIG. 4. (Color online) The topography line profiles measured along the [001] direction for (a) Mn1 and Mn2 on GaAs(110) surface and for (b) Cd1 and Cd2 on the respective GaP($1\bar{1}0$) and GaP(110) surface planes. The maximum of each topography profile representing the approximate dopant position was set to the origin (0 nm). (c) and (d) show the line profiles both through the (A) center and (B) off center (2.0 nm) of the corresponding envelopes measured along the [001] direction.

surface acceptors, we associate a dramatic reduction of the contrast symmetry around the surface normal from a slightly broken C_{2v} to a clear C_s symmetry with the cleavage induced broken symmetry of the crystal surface.

Figures 3(c) and 3(d) show the FFT processed contour plots of the Cd induced envelopes on GaP($1\bar{1}0$) and GaP(110) surface planes, respectively. The measured LDOSs around Mn and Cd acceptors are further shown by line profiles through both the center and a point off center of the envelope images [Figs. 4(f) and 4(d)]. The off-center line profiles, which are parallel to the envelope main axis along the [001] direction, were acquired at a distance about 2.0 nm away from each envelope maximum. As determined by the unoccupied state imaging mode and the central line profiles, the maximum of the Cd1 envelope shifts away laterally along the [00$\bar{1}$] direction on the GaP($1\bar{1}0$) plane. A similar shift for the Cd2 envelope occurs toward the [001] direction on the GaP(110) plane with respect to the maximum of the topographic dopant position. The shift of the envelope is somewhat bigger for the near-surface acceptors. For example, the lateral shift for Cd1 was measured to be around 28% more than the one for Cd2, and for Mn1 and Mn2, this difference is about 16% on the same surface plane. This clearly indicates that the shift of the contrast maximum has a dependence on the dopant depth. A similar depth dependent contrast shift has previously been observed for Zn acceptors on the (110)-cleavage surface of *p*-type GaAs.[17] Unlike the case for the Mn envelopes [Fig. 4(c)], the off-center line profiles of the Cd envelopes revealed additional fine structures appearing as weak protrusions in the middle of both

upper and lower edges [Fig. 4(d)]. For example, these Cd induced protrusions, which are also visible in the envelope images [Figs. 3(c) and 3(d)], extend sideways along GaP[$1\bar{1}0$] and GaP[$\bar{1}10$] in opposite directions on GaP(110) plane. The observed protrusions make a minor contribution to the anisotropic appearance of the Cd LDOS at large distances, but have no dependence either on the opposite orientation of the surface states at two orthogonal crystal facets or on the spatial position of the dopant center.

IV. THEORETICAL COMPARISON

A. Tight-binding model

We used a multiband tight-binding Hamiltonian and the approach developed in Ref. 11 to calculate the ground state wave function of Mn and Cd acceptor states in GaAs and GaP hosts, respectively. The calculations are performed for isolated bulklike acceptors, with the actual binding energies of either 102 meV (for Cd) or 113 meV (for Mn). The tight-binding parameters for the host materials come from Ref. 18. As in Ref. 11, the effective potential is considered to arise from the hybridization of the As *p* orbitals with the Mn or Cd *d* orbitals on site. This produces an effective spin-dependent potential on the nearest-neighbor As atoms to the magnetic Mn dopant, and an effective spin-independent potential on the nearest-neighbor P atoms to the nonmagnetic Cd dopant. The parameters used for Mn:GaAs are those described in Ref. 19, whereas for Cd:GaP, a single parameter, 2.508 eV, is used for the potential at the Cd site and at the four neighboring P sites.

The spatial plots of the calculated LDOS based on the TBM are shown in logarithmic scale in Figs. 5(a) and 5(b)
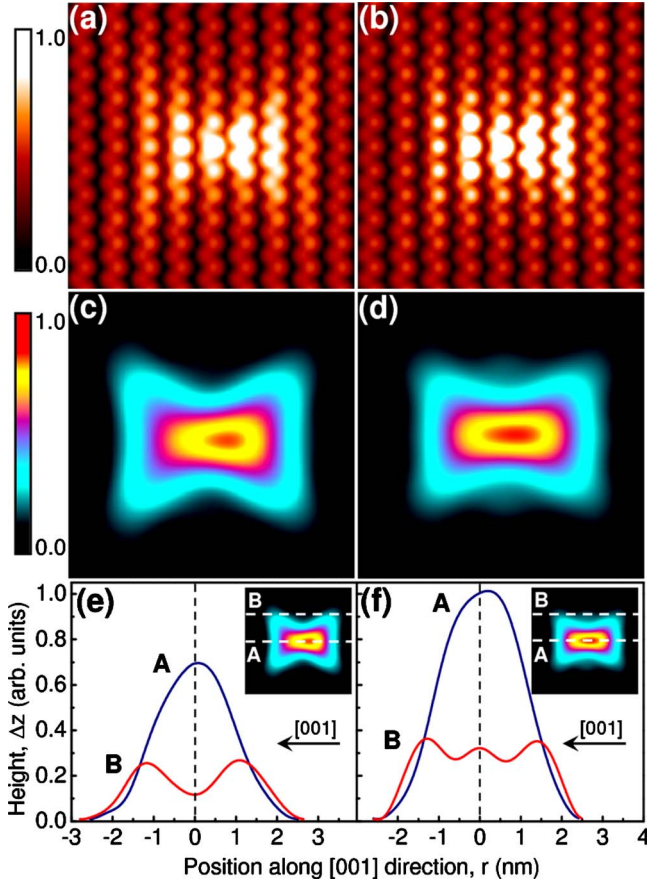
FIG. 5. (Color online) Cross-sectional TBM view of (a) Mn LDOS on GaAs(110) and (b) Cd LDOS on GaP(110) plane. The center of each Mn and Cd acceptor states is located five atomic layers below the (110) viewing plane. The spatial extent of the atomic orbitals is set to half of the nearest-neighbor bond length. (c) and (d) show the corresponding contour plots of the envelope images. The size of each frame is 5×5 nm^2. The line profiles measured both through the (A) center and (B) off center (1.5 nm) of (e) Mn and (f) Cd envelopes along the [001] direction. The measured heights were normalized by the maximum value of the Cd envelope.

for Mn:GaAs and Cd:GaP states, respectively. The frames depict the cross section of the LDOS for both acceptors on the (110) plane, with each of the acceptors located at the same spatial position (5 ML below the viewing plane) in the corresponding crystal. Consistent with the X-STM results, the calculations reveal very similar spatially extended anisotropic crosslike structures for both of the Mn and Cd wave functions. The cross sections in the (110) plane display symmetry in the $(1\bar{1}0)$ mirror plane and a relatively weak asymmetry in the [001] direction (C_{2v} symmetry). For a precise analysis of the TBM data, the high-frequency (Bloch state) component is filtered out from the topography using a low-pass FFT filter. As shown in Figs. 5(c) and 5(d), the spatial structure and symmetry of the Cd envelope in GaP appear slightly different from those of Mn in GaAs. The apparent difference has different features depending on whether the observation point is a short or long distance from the envelope maximum. The symmetry of the LDOS near the center

of Mn envelope is found to be strongly lowered with respect to either GaAs($1\bar{1}0$) or GaAs(001) reflection planes. However, the LDOS around the Cd envelope maximum exhibits almost a complete symmetric profile with the short axis under the same GaP reflection planes. The change of the symmetry around the core of the acceptor envelope can be associated with the structural differences between the $3d$ atomic orbital components of magnetic and nonmagnetic acceptors. For instance, the Cd acceptor has a fourfold degeneracy (angular momentum of 3/2), whereas Mn introduces a threefold degenerate state (angular momentum of 1). In agreement with the experimental results, the envelope obtained from the calculated Cd LDOS in GaP reveals the presence of weak protrusions both at the upper and lower edges and also the right and left corners of the related envelopes. The observed fine features, which were characterized quantitatively by the line profiles [Fig. 5(f)], extend spatially sideways along the $(1\bar{1}0)$ mirror plane.

B. Envelope-function effective-mass model

To further analyze the effect of the SO interaction on the Cd and Mn LDOSs, we also performed EM calculations within the zero-range potential approximation.[20] For strong SO interaction, the Hamiltonian of the fourfold degenerate Γ_8 topmost valence band can be expressed in the following form:

$$H_{\Gamma_8} = \left(\gamma_1 + \frac{5}{2}\gamma_2\right)k^2 - 2\gamma_2\sum_i J_i^2 k_i^2 - 2\gamma_3\sum_{i<j} k_i k_j \{J_i J_j\}, \quad (1)$$

where γ_1, γ_2, and γ_3 are the Luttinger-Kohn (LK) parameters and J is the angular momentum matrix for 3/2 state. It is well known[21] that the Hamiltonian (1) is the upper-left (4×4) part of the (6×6) Hamiltonian, which is obtained by performing the unitary transformation of the block-diagonal Hamiltonian with the (3×3) blocks on the diagonal and adding the value of the spin-orbit splitting ΔE_{so} to the last two diagonal terms:

$$H_{\Gamma_{15}} = (\alpha_1 + 2\alpha_2)k^2 - 4\alpha_2\sum_i I_i^2 k_i^2 - 4\alpha_3\sum_{i<j} k_i k_j \{I_i I_j\}. \quad (2)$$

When $\Delta E_{so}=0$ (or small enough to neglect it), the Hamiltonian (2) describes the Γ_8 valence band and the Γ_7 split-off band as well as their interaction. For large SO splitting, one can use Eq. (1) as the Hamiltonian of the Γ_8 band only. The connection between the constants γ_i [Eq. (1)] and α_i [Eq. (2)] is determined by comparing Eqs. (1) and (2), and is written as

$$\gamma_1 = \alpha_1 - \frac{2}{3}\alpha_2, \quad \gamma_2 = \frac{2}{3}\alpha_2, \quad \gamma_3 = \frac{2}{3}\alpha_3. \quad (3)$$

To model the ground state wave function of Mn:GaAs and Cd:GaP acceptors in the case of strong and weak SO coupling, we numerically solved both Eqs. (1) and (2) within the cubic approximation ($\gamma_2 \neq \gamma_3$) for a zero-radius potential. In these calculations, the LK parameters[22] for the $J=3/2$ state, GaAs$_{\Gamma_8}$ ($\gamma_1=7.65$, $\gamma_2=2.41$, and $\gamma_3=3.28$) and
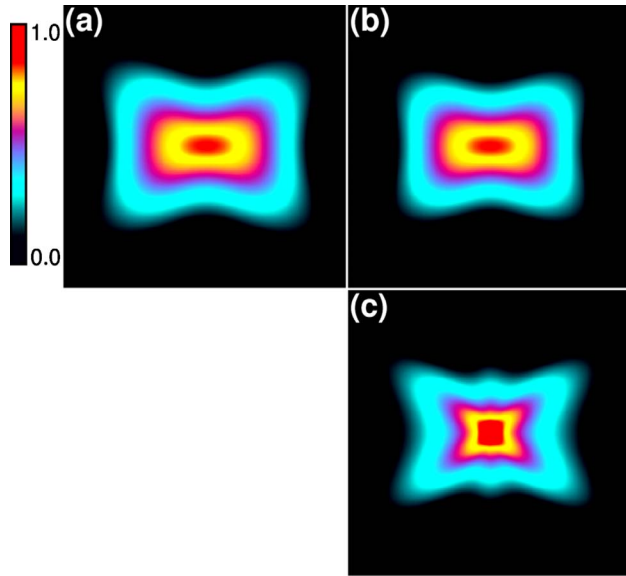
FIG. 6. (Color online) The cross-sectional view of logarithmic scale absolute value of the calculated hole ground state probability density $|\Psi_j|^2$ for (a) Mn:GaAs and (b) Cd:GaP obtained from a four-band LK model for the case of $\Delta E_{so} \neq 0$, and for (c) Cd:GaP obtained from a six-band LK model for the case of $\Delta E_{so} \approx 0$. The size of each frame is 5×5 nm^2.

GaP$_{\Gamma_8}$ ($\gamma_1 = 4.20$, $\gamma_2 = 0.98$, and $\gamma_3 = 1.66$), and for the $J = 1$ state, GaP$_{\Gamma_{15}}$ ($\gamma_1 = 5.18$, $\gamma_2 = 1.47$, and $\gamma_3 = 2.49$), were taken into account. We analyzed the bulklike acceptor state with a given binding energy of $E_a = 100$ meV, and compared quantitatively the corresponding logarithm of the ground state probability density both in the presence and in the absence of the split-off bands.

The contour plot of the calculated cross sections for the logarithmic scale acceptor LDOS in the GaAs(110) and GaP(110) atomic planes is shown in Fig. 6. As can be seen in Figs. 6(a) and 6(b), the results obtained by the four-band approach revealed a similar anisotropic structure to the acceptor LDOS with a slightly different localization radius for each of the Mn:GaAs and Cd:GaP wave functions. However, the profile in Fig. 6(c) exhibits striking additional fine features extending in the [001] and [$1\bar{1}0$] directions as seen before in the analysis of the experimental and TBM results. One can clearly see that all the images have the same C_{2v} symmetric character, whereas the fine structure in Fig. 6(c) for the Γ_{15} Hamiltonian [Eq. (2)] is more pronounced than that of Eq. (1).

The observed additional fine protrusions in the upper and lower edges of the Cd LDOS can be explained based on the EMM. The zero-range approximation for a dopant potential, which applies to distances larger than the core potential radius, will be applied to clarify the difference between acceptor wave functions calculated using the Hamiltonian of Eq. (1) and those calculated using the Hamiltonian of Eq. (2). In the zero-range approximation, the acceptor wave function is formed as a solution of $(H - IE)\Psi = V$ in the k representation.[20] As was mentioned above, Hamiltonian (1) is a part of Hamiltonian (2). In other words, Eq. (2) provides all solutions that are similar to those of Eq. (1), but the reverse is not true. For Eq. (1), this set of equations is effectively reduced to two equations due to Kramers degeneracy. The solution for a spinor component in the k representation displays a d-like spherical harmonic centered at the dopant core. The solution of Eq. (2) is similar; however, it includes even higher order spherical harmonics (of at least g-like character). Consequently, the image of an acceptor in a semiconductor with small SO splitting like GaN will produce a richer spatial structure, but the overall shape anisotropy will be conserved.

V. CONCLUSIONS

The wave functions of holes bound to a Mn acceptor in GaAs and a Cd acceptor in GaP are spatially mapped and investigated at room temperature by cross-sectional scanning tunneling microscopy. Similar to the Mn state in GaAs, we found a highly anisotropic, crosslike contrast for Cd on the GaP(110) cleavage plane. As determined by the topographic measurements, the SO interaction in the host material does not yield any significant change in the acceptor shape anisotropy, whereas the symmetry of the hole wave function is only influenced strongly by the spatial position of the dopant atom with respect to the host surface plane. The experimentally obtained results demonstrate that the principal determinant of the acceptor induced anisotropic shape of the LDOS in III–V semiconductors is solely the cubic symmetry of the host crystal and not the SO interaction, as previously suggested by tight-binding calculations.[7,11] We confirmed this by obtaining similar crosslike spatial structures for the acceptor ground state wave function using tight-binding and envelope-function effective-mass models, including either finite or zero SO terms in the model calculations. Nevertheless, our experiments and theoretical models also revealed that a strong reduction of the SO interaction gives rise to additional fine structure in the acceptor state wave functions. These fine structures appear as weak protrusions at the side edges of the acceptor envelopes and make a negligible contribution to the overall acceptor LDOS.

[1] B. E. Kane, Nature (London) **393**, 133 (1998).

[2] *Semiconductor Spintronics and Quantum Computation*, edited by D. D. Awschalom, N. Samarth and D. Loss (Springer-Verlag, Heidelberg, 2002).

[3] H. Sellier, G. P. Lansbergen, J. Caro, S. Rogge, N. Collaert, I. Ferain, M. Jurczak, and S. Biesemans, Phys. Rev. Lett. **97**, 206805 (2006).

[4] J.-M. Tang, J. Levy, and M. E. Flatté, Phys. Rev. Lett. **97**, 106803 (2006).

[5] H. Ebert and G. Schütz, *Spin-Orbit Influenced Spectroscopies of Magnetic Solids* (Springer, Heidelberg, 1996).

[6] J. F. Zheng, X. Liu, N. Newman, E. R. Weber, D. F. Ogletree, and M. Salmeron, Phys. Rev. Lett. **72**, 1490 (1994).

[7] A. M. Yakunin, A. Y. Silov, P. M. Koenraad, J. H. Wolter, W. Van Roy, J. De Boeck, J.-M. Tang, and M. E. Flatté, Phys. Rev. Lett. **92**, 216806 (2004).

[8] J. Schneider, U. Kaufmann, W. Wilkening, M. Baeumler, and F. Kohl, Phys. Rev. Lett. **59**, 240 (1987).

[9] M. Linnarsson, E. Janzén, B. Monemar, M. Kleverman, and A. Thilderkvist, Phys. Rev. B **55**, 6938 (1997).

[10] F. Marczinowski, J. Wiebe, J.-M. Tang, M. E. Flatté, F. Meier, M. Morgenstern, and R. Wiesendanger, Phys. Rev. Lett. **99**, 157202 (2007).

[11] J.-M. Tang and M. E. Flatté, Phys. Rev. Lett. **92**, 047201 (2004).

[12] J.-M. Tang and M. E. Flatté, Phys. Rev. B **72**, 161315(R) (2005).

[13] E. F. Schubert, *Doping in III–V Semiconductors* (Cambridge University Press, Cambridge, England, 1993).

[14] O. Madelung, *Semiconductors-Basic Data*, 3rd ed. (Springer, New York, 2004).

[15] R. de Kort, M. C. M. M. van der Wielen, A. J. A. van Roij, W. Kets, and H. van Kempen, Phys. Rev. B **63**, 125336 (2001).

[16] G. Mahieu, B. Grandidier, D. Deresmes, J. P. Nys, D. Stiévenard, and P. Ebert, Phys. Rev. Lett. **94**, 026407 (2005).

[17] S. Loth, M. Wenderoth, L. Winking, R. G. Ulbrich, S. Malzer, and G. H. Döhler, Jpn. J. Appl. Phys., Part 1 **45**, 2193 (2006).

[18] D. J. Chadi, Phys. Rev. B **16**, 790 (1977).

[19] A. M. Yakunin *et al.*, Nat. Mater. **6**, 512 (2007).

[20] A. Monakhov, K. Romanov, I. Panaiotti, and N. Averkiev, Solid State Commun. **140**, 422 (2006).

[21] G. L. Bir and G. E. Pikus, *Symmetry and Strain-Induced Effects in Semiconductors* (Halsted, Jerusalem, 1974).

[22] A. Baldereschi and N. O. Lipari, Phys. Rev. B **8**, 2697 (1973).